

Collision avoidance method of autonomous vehicle based on improved artificial potential field algorithm

Proc IMechE Part D:

J Automobile Engineering

1–15

© IMechE 2021

Article reuse guidelines:

sagepub.com/journals-permissions

DOI: 10.1177/09544070211014319

journals.sagepub.com/home/pid

Song Feng¹ , Yubin Qian¹ and Yan Wang²

Abstract

Both emergency braking and active steering are possible choices for collision avoidance manoeuvres, and any obstacle avoidance strategy aims to design a control algorithm preventing accidents. However, the real-time path needs to consider the motion state of surrounding participants on the road. This work presents a collision avoidance algorithm containing the path-planning and the tracking controller. Firstly, the lateral lane-changing spacing model and the longitudinal braking distance model are presented, describing the vehicle to reactively process dynamic scenarios in real environments. Then, we introduce the safety distance into the artificial potential field algorithm (APF), thereby generating a safe path in a simulated traffic scene. Redesigning the influence range of obstacles based on the collision areas and corresponding safety distance compared with the classic APF. Besides, based on the threat level, the repulsion is divided into the force of the position repulsion and the speed repulsion. The former is related to the relative position and prevents the vehicle from approaching the obstacle. The latter is opposite to the relative speed vector and decelerates the ego vehicle. Simultaneously, the attraction is improved to apply a dynamic environment. Finally, we design a model predictive control (MPC) to track the lateral motion through steering angle and a Fuzzy-PID control to track the longitudinal speed, turning the planned path into an actual trajectory with stable vehicle dynamics. To verify the performance of the proposed method, three cases are simulated to obtain the vehicle responding curves. The simulation results prove that the active collision avoidance algorithm can generate a safe path with comfort and stability.

Keywords

Autonomous vehicle, collision avoidance algorithm, safety distance, path planning, tracking control

Date received: 14 January 2021; accepted: 31 March 2021

Introduction

Traffic accidents are a significant cause of human death and traffic congestion, and over 90% of car crashes are generated by human errors.¹ The autonomous vehicle is considered as a solution for modern intelligent transport, improving traffic safety and reducing the burden of drivers.² However, if the autonomous car is used to replace human drivers, it needs to be intelligent enough to deal with complicated traffic scenarios. Key collision avoidance technologies include perception, behavioural decision, path planning and path tracking.³ In the perception module, the data from various sensors, including Lidar, camera, GPS, etc., are fused to obtain corresponding information. In recent years, vehicle-to-vehicle (V2V) communication allows the cars to connect, obtaining the state about other vehicles.⁴ Furthermore, vehicle-to-everything (i.e. vehicle-to-vehicle and vehicle-to-infrastructure) is the crucial

technology of the future intelligent transportation system; information shared among traffic participants can be more abundant and with higher quality than sensors.⁵ This research will address planning the safe collision avoidance trajectory in a dynamic environment to achieve better vehicle performance, deeming the ego

¹School of Mechanical and Automotive Engineering, Shanghai University of Engineering Science, Shanghai, China

²SAMR Defective Product Administrative Center, Beijing, China

Corresponding authors:

Yubin Qian, School of Mechanical and Automotive Engineering, Shanghai University of Engineering Science, Songjiang Campus 8B 601, Shanghai 201620, China.

Email: qianyb@sues.edu.cn

Yan Wang, SAMR Defective Product Administrative Center, Beijing 100101, China.

Email: wangyan@dpac.gov.cn

vehicle can accurately receive demanded information through various sensors and wireless communication.

The path planning section is a crucial subject in autonomous vehicles, and the primary purpose is to design a safe path without collision. Although the algorithms for obstacle avoidance have been widely researched in robots and unmanned aerial vehicles (UAV),⁶ it is inappropriate to apply these algorithms to traffic scenarios ignoring the road regulations and vehicle dynamics. Thus, the traditional algorithm should be improved to apply the traffic environment (i.e. we should also consider the safe distance between the ego vehicle and surrounding objects). At present, the main algorithms contain map-based methods, sampling-based algorithms and the artificial potential field (APF).

A* algorithm is extensively used as a map-based method in the shortest path planning, which divides the map into grids and estimates all reachable nodes gaining the ideal path based on a cost function. Nevertheless, the A* algorithm is not reasonably suitable in a dynamic environment. To solve the moving obstacle, Ferguson *et al.* proposed an Anytime Dynamic A*(AD*) algorithm using the A* attributes to generate solutions. However, the heuristic method is challenging to be found.⁷ In 2007, an autonomous car produced by Stanford University used an improved A* algorithm in the DARPA Urban Challenge.⁸ Pang *et al.*⁹ proposed a new A* algorithm with equal-step sampling, which is suitable for a dynamic environment and resolves the path planning on curved roads.

The rapidly-exploring random tree algorithm (RRT) is a sampling-based search method. The RRT explores the entire environment by randomly creating nodes in space and quickly reducing the distance between the nodes and the tree.¹⁰ To reduce calculation time and apply it to an autonomous vehicle, Lan and Cairano¹¹ proposed a two-way RRT algorithm to plan a safe lane-changing path. They sampled at the start point and the goal point simultaneously, making the path generation directional to a certain extent and improving the efficiency. Shi *et al.*¹² proposed an improved RRT algorithm with a turning angle constraint to solve large randomness, slow convergence speed and deviation. Besides, due to the excellent applicability in a high-dimensional space, the RRT algorithm is also used in UAV path planning. For instance, Lin and Saripalli¹³ set up reachable sets instead of single points to predict moving obstacles and combine these sets with RRT to generate a real-time path. However, the planned path created by A* and RRT is not continuous, which means it often needs to be smoothed by the spline curves,¹⁴ Bezier curves¹⁵ and polynomial curves.¹⁶

The APF sets up the potential fields (PFs) of obstacle and destination to produce the repulsion and attraction, so the path extends along the descent direction of the total PF. Because of simplicity and elegance, the APF could satisfy real-time control requirements.¹⁷ Now, many researchers apply the improved APF to

autonomous vehicles.¹⁸ A feasible method is to introduce a distance model into the APF. For instance, Gao *et al.*¹⁹ proposed a conditional artificial potential field (C-APF) in the mixed traffic scenario that performs the lane-changing at a safe distance. Wang *et al.*³ redefined the repulsive field range of obstacles as an ellipse according to drivers' behaviours. Then, the feasibility of the improved algorithm was verified through co-simulation and real car tests. In addition to improving the algorithm, the combination with optimal control is another workable solution. In this method, obstacles and road boundaries are defined as constraints, so a model predictive controller (MPC) contains both planning and control functions with vehicle dynamics. Ji *et al.*²⁰ introduced a 3-D virtual dangerous PF of road and obstacles, and the multi-constrained model predictive controller (MMPC) is defined to control the front steering angle. Huang *et al.*²¹ divided the process into virtual space and actual space, where the former evaluates the predicted path and the latter generates a feasible trajectory. Besides, the APF algorithm is also widely used in UAV. To minimize the impact on the surrounding area environment, Du *et al.*²² proposed a real-time collision avoidance strategy based on the dynamic artificial potential field (DAPF) algorithm. However, both methods have certain drawbacks. The collision avoidance behaviours include active steering and deceleration braking, so a single safety distance introduced in the APF algorithm cannot fully describe the complete process. Path planning with dynamic constraints can make the controller track the desired path stably, but it inevitably leads to a complicated calculation. To sum up, the classic APF has significant advantages in coping with real-time collision avoidance, but it needs to be improved for traffic environments.

Then, the tracking controller is an indispensable part of a collision-avoidance system, and its purpose is to ensure the autonomous vehicle follows the planned path stably and safely.²³ At present, tracking control can be divided into lateral research (i.e. steering control) and longitudinal research (i.e. speed control). For instance, Wang *et al.*²⁴ adaptively weighted the cost function based on the fuzzy logic to improve the MPC controller. In Lihan *et al.*,²⁵ a fuzzy-PID adjusted the control parameters online, reducing random interference and tracking the longitudinal speed. However, lane-keeping and lane-changing are both alternatives to avoid car collision, which means the combination control in the lateral and longitudinal direction is necessary. In previous studies, Wang *et al.*²⁶ combined a multi-objective adaptive cruise control (ACC) and a hierarchical algorithm to realize the tracking problem. Cao *et al.*²⁷ proposed an active collision-avoidance system integrated with a lateral path following module and a fuzzy longitudinal following module. Wang *et al.*²⁸ proposed a motion planning method to mitigate the crash if the collision is unavoidable, then the designed MPC algorithm to control the front wheel steering and longitudinal speed.

Overall, traffic accidents on roads are mostly caused by car crashes, and any obstacle avoidance strategy aims to design a control algorithm preventing accidents.²⁰ The contribution of this paper is to design an improved APF method for generating a safe and stable collision-free path in a dynamic traffic environment. On the one hand, two proposed safety distance models are introduced into the improved algorithm according to different collision areas. So the influence range of obstacles is determined by the position, speed and direction, which is no longer a fixed value compared with a conventional algorithm. On the other hand, based on different obstacles (the threat level is determined by the mass, size and speed), the proposed position repulsion works to prevent collision accidents, and the defined speed repulsion decelerates the autonomous vehicle when necessary. The improved attraction defines the global attraction and speed attraction based on the influence range of the dynamic obstacles. The planned path is then controlled by the lateral and longitudinal tracking module and simulated in different proposed scenarios.

The rest of this paper is organized as follows. Section II establishes the safety distance model under different collision avoidance behaviours (i.e. active steering and emergency braking). Section III proposes the improved APF algorithm. Section IV designs the tracking controller to ensure stable vehicle dynamics. Section V verifies the feasibility of the proposed collision avoidance algorithm in simulated scenarios. Section VI puts forward the conclusions.

Safety distance model

The current path planning algorithm is to search for a safe route on the global path. However, the process is usually reduced to the movement of particles. Then the tracking controller ensures the vehicle meets dynamic constraints to form an actual motion trajectory. If the algorithm ignores the safety distance, the occurrence of collision in realistic scenarios will increase. A lane-changing initial spacing model and a longitudinal braking distance model are established in this section to plan the collision avoidance path of the vehicle.

Lane-changing initial spacing model

Lateral control (i.e. active steering only) is an operation for collision avoidance manoeuvre.²⁹ In this paper, time to collision (TTC) is utilized as the index to establish the lane-changing initial spacing model. Figure 1 shows a two-lane road model embracing one current lane and one adjacent lane. Where E is the ego vehicle driving in the current lane, F and R are surrounding vehicles in the adjacent lane, and OB denotes the obstacle vehicle in the current lane.

As a lateral motion state, it must guarantee the successful lane-changing of E without disturbing other participant R and F . As shown in Figure 1, we should

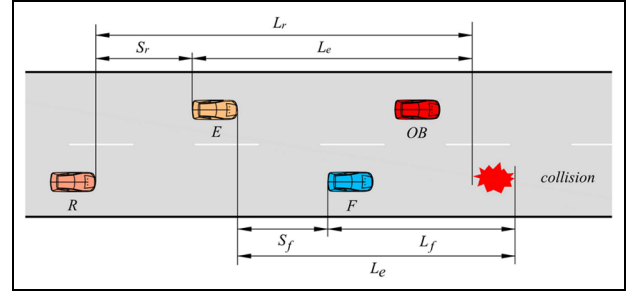


Figure 1. Lane-changing distance model.

maintain a specific initial spacing S_r before E changes lane. Otherwise, E is prone to occur a rear crash with R . On the rear of E , the distance condition is as follows:

$$S_r > L_r - L_e \quad (1)$$

Where subscript r means the rear vehicle, the subscript e means the ego vehicle, L is the longitudinal displacement. In the previous study, since the driver who wanted to change lane maintain a constant speed in the longitudinal direction, the critical factors of this process are reflected in the velocity, the lane-changing time, and the longitudinal distance.³⁰ The displacement difference between R and E can be expressed explicitly as:

$$\Delta L_1 = (v_r - v_e)t + \int_0^t \int_0^t a_r(\tau) d\tau dt \quad (2)$$

Where v is the longitudinal velocity, t denotes the time from the beginning of lane-changing to the current moment ($t \leq \text{TTC}$), and $a(\tau)$ is the longitudinal acceleration (deceleration) of R . The relationship between velocity and TTC can be obtained from the literature.³¹

The safety of the ego vehicle is controllable by the rear vehicle. If ΔL_1 is positive, R will continue to approach E in the time interval $(0, t)$. To ensure safe lane-changing, the initial spacing S_r must meet certain conditions according to equation (1). Otherwise, E is not allowed to manipulate a steer. If ΔL_1 is negative, it means that E is edging away from R . Note that, the case $L_e \approx L_r$ resembles returning to the original lane after overtaking, S_r should be regarded as the minimum braking distance of the rear vehicle. If $\Delta L_1 = 0$, the lane-changing conditions will not be available, so E also must give up the steering. Equation (2) is improved as follows:

$$S_r = \begin{cases} \Delta L_1 + v_r t_0, & L_e < L_r \\ \frac{v_r^2}{2a_{br}} + d_0 + v_r t_0, & L_e \geq L_r \end{cases} \quad (3)$$

Where t_0 is the reaction time before taking braking measures,³⁰ a_{br} is the maximum vehicle braking deceleration of R , d_0 denotes the ideal clearance when two vehicles brake to a standstill.

The position between E and F is also essential when changing lane. Since the safety of the front vehicle F is controllable by the ego vehicle,³² if the front vehicle

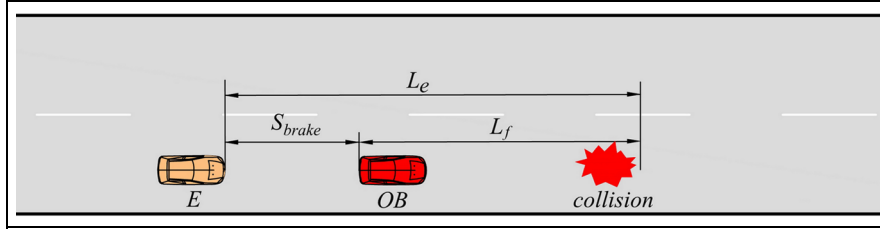


Figure 2. Longitudinal braking distance model.

decelerates suddenly, a specific initial spacing S_f to be reserved, preventing collision:

$$S_f > L_e - L_f \quad (4)$$

Where subscript f means the front vehicle, we can express the displacement difference between F and E as:

$$\Delta L_2 = (v_e - v_f)t + \int_0^t \int_0^t a_f(\tau) d\tau dt \quad (5)$$

Similarly, the improved initial spacing S_f can be further expressed as:

$$S_f = \begin{cases} \Delta L_2 + v_e t_0, & L_f < L_e \\ \frac{v_e^2}{2a_{be}} + d_0 + v_e t_0, & L_f > L_e \end{cases} \quad (6)$$

Where a_{be} is the maximum vehicle braking deceleration of E . In reality, a single spacing model is not suitable for mixed traffic scenarios,¹⁹ which means the preceding and the following vehicle could exist in the adjacent lane simultaneously. So, the initial spacing of lane-changing is defined as:

$$S_{steer} = \max \{S_r, S_f\} \quad (7)$$

Longitudinal braking distance model

When the ego vehicle fails to avoid collision through active steering, longitudinal control (i.e. emergency braking) will be another essential choice.²⁹ In reality, vehicle braking performance is limited by the initial speed, braking system and road adhesion coefficient *et al.* Assuming the braking system can exert its maximum effectiveness, the longitudinal braking distance model is shown in Figure 2.

For lane-keeping, the ego vehicle adaptively follows the obstacle vehicle ahead. If an emergency occurs, for the ego vehicle to conduct safe collision avoidance by controlling longitudinal velocity, the braking distance S_{brake} is derived:

$$S_{brake} = \frac{v_e^2}{2a_{be}} + (v_e - v_{ob})T_t - \frac{v_{ob}^2}{2a_{ob}} \quad (8)$$

Where v_{ob} is the velocity of OB , a_{ob} is the maximum braking deceleration of OB and T_t is the time delay of the braking system.³³

Path planning

This section introduces the path planning method of the proposed collision avoidance algorithm.

The traditional APF algorithm

The APF was proposed by Khatib³⁴ in the 1980s, and the traditional algorithm proposed two virtual potential fields. One is an attractive field; it provides an attraction for the goal point guiding the robot towards its destination. The other is a repulsive field that exerts the repulsion, preventing collision between the robot and the obstacle.²² The two potential fields can be expressed as:

$$U_{att} = \frac{1}{2} k_{att} \rho_g^2 \quad (9)$$

$$U_{rep} = \begin{cases} \frac{1}{2} k_{rep} \left(\frac{1}{\rho} - \frac{1}{\rho_0} \right)^2, & \rho \leq \rho_0 \\ 0, & \rho > \rho_0 \end{cases} \quad (10)$$

Where U_{att} and U_{rep} are the attraction field and the repulsive field, k_{att} and k_{rep} are the gain coefficient of the attraction and the repulsion, ρ_g is the distance from the robot to the goal point, ρ is the distance from the robot to the obstacle, ρ_0 is the repulsive influence range of the obstacle. The attraction and repulsion can be obtained by the gradient descent method, which can be expressed as:

$$F_{att} = -\nabla U_{att} = k_{att} \rho_g \quad (11)$$

$$F_{rep} = -\nabla U_{rep} = \begin{cases} \frac{k_{rep}}{\rho^2} \left(\frac{1}{\rho} - \frac{1}{\rho_0} \right), & \rho \leq \rho_0 \\ 0, & \rho > \rho_0 \end{cases} \quad (12)$$

Therefore, the robot moves from the starting point to the goal point under the resultant force of attraction and repulsion. However, as a path planning algorithm for the robot, the repulsive force has a constrained range of action, and it merely acts within the fixed domain ρ_0 .

Road potential field

In the earth coordinate system (X, O, Y), marking lines of the road model defined in Figure 3 are divided into two boundary lines and one centreline. Autonomous vehicles must be constrained by traffic regulations: (a) in the absence of obstacles, the vehicle should follow

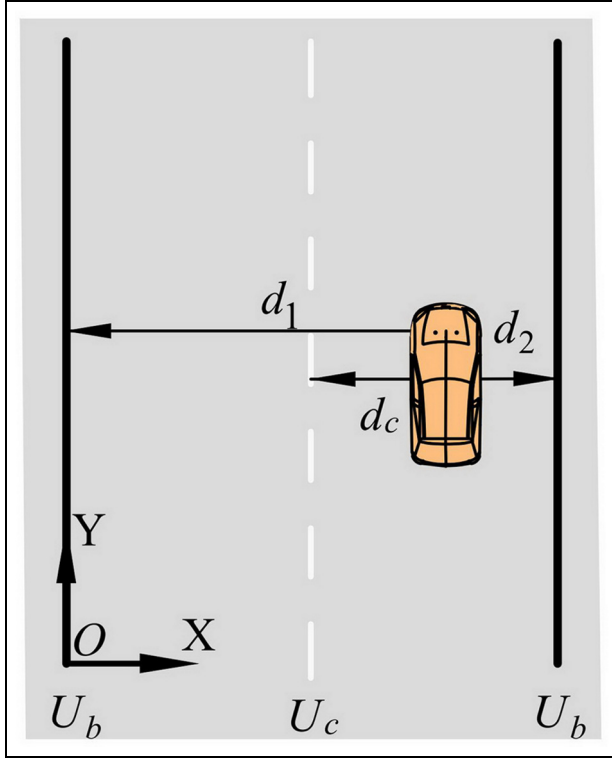


Figure 3. Road model. XOY represents the earth coordinate system.

the centre of the lane; (b) during collision avoidance, the vehicle neither collides with obstacles nor drives out boundaries.

The total PF of the road can be expressed as:

$$U_{road} = U_b + U_c \quad (13)$$

U_b and U_c are the PF of road boundaries and road centreline. In detail, once the autonomous vehicle approaches the position of boundaries, U_b should increase rapidly and reach the maximum so that it can prevent the vehicle from driving out of the edges:

$$U_b = k_{b1} \frac{1}{d_1^2} + k_{b2} \frac{1}{d_2^2} \quad (14)$$

Where K_{b1} and K_{b2} are coefficients of two road boundaries, d_1 and d_2 represent the distance of the vehicle to the left and right boundary, respectively. Then, U_c ought to work with U_b keeping the autonomous vehicle in the centre of the current lane. In other words, the PF of the road centreline should be small enough to be easily overcome if a lane-changing is necessary.²⁰ Referring to the expression of Gaussian function,⁵ we present the PF of the road centreline as follows:

$$U_c = k_c e^{-\frac{d_c^2}{2\sigma_c^2}} \quad (15)$$

Where k_c is the coefficient of road centreline, σ_c is the convergence coefficient of road width, d_c is the distance from the vehicle to road centreline. Figure 4 shows the three-dimensional graphical representation

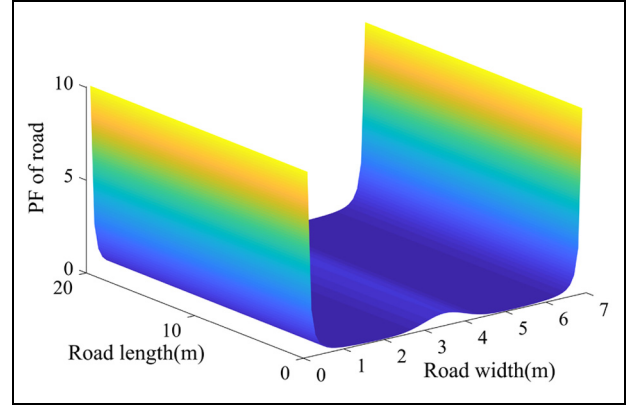


Figure 4. The three-dimensional potential field of the road.

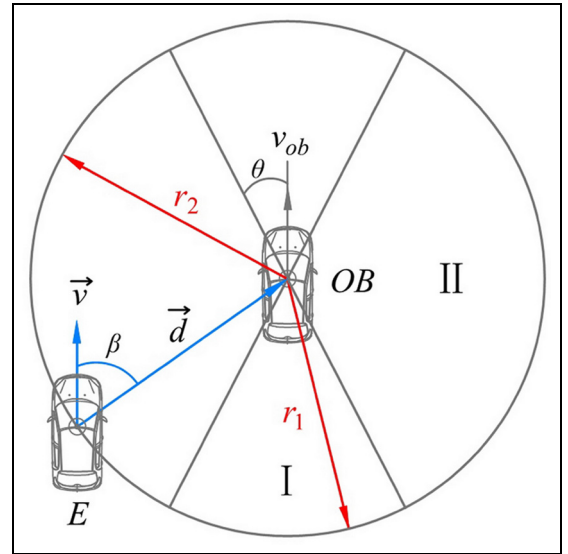


Figure 5. Influence range of obstacle based on safety distance.

of the road PF. It has good symmetry characteristics that contain the maximum value at road boundaries, an appropriate value at the road centreline, and the minimum value at the lane's centre.

The relationship between the PF and the force is obtained by the gradient descent method:

$$F_{road} = -\nabla U_{road} \quad (16)$$

Influence range based on safety distance

The influence range of obstacles defines the region of repulsive force. The traditional APF algorithm sets it to a fixed value, which does not match the realistic environment. In this paper, how to convert the calculated safety distance into the influence range is a critical consideration. As shown in Figure 5, the collision area is split into two regions: I and II, for the car-car collision. The rear crashes or the frontal crashes are prone to occur in zone I, and the most severe risk happens

around 1/3 overlap crashes.³⁵ Furthermore, the side crashes cause high mortality and should be avoided in zone II.²⁸ Consider the above cases, the influence range r_I and r_{II} are adjusted according to the braking distance and the lane-changing initial spacing, respectively.

In Figure 5, v is the relative speed vector between the vehicle and the obstacle, d is the relative position vector between the vehicle and the obstacle, β is the relative angle vector between the relative speed and the relative position, θ represents the crash angle corresponding to the 1/3 overlap crashes. Previous research recognized the response parameters of stable steering as essential indicators.³⁶ Since the algorithm takes the vehicles as the research object, ρ_0 set in the classic APF is redefined as the minimum turning radius, referring to the two-wheel steering model and uniform circular motion.¹⁰

$$\rho_0 = \frac{v}{\omega_r} = \frac{L(1 + Kv^2)}{\delta_{\max}} \quad (17)$$

Where v is the relative speed, ω_r is the yaw angular velocity, L is the distance from the front wheel to rear wheel, σ_{\max} is the maximum steering angle, K characterizes the steering stability performance named the stability factor:

$$K = \frac{m}{L} \left(\frac{a}{k_2} - \frac{b}{k_1} \right) \quad (18)$$

Where m is the mass of the ego vehicle, a and b are the distance from the front wheel and rear wheel to the centre of mass, k_1 and k_2 are the cornering stiffness values of the front and rear tires. The braking distance defined should be maintained to plan a safe path in zone I, and the minimum turning radius is appropriately extended by the distance coefficient. The influence of obstacle r_I can be expressed as:

$$r_I = S_{brake} + k_b \rho_0 \quad (19)$$

Where k_b is the distance coefficient in zone I, since vehicle and obstacle are prone to side crash in part II, the value of r_{II} also can be defined based on the lane-changing initial spacing and expended turning radius as follows:

$$r_{II} = S_{steer} + k_s \rho_0 \quad (20)$$

Where k_s is the distance coefficient in zone II, in order to limit the maximum range, we defined an influence distance threshold r_{\max} can be expressed as:

$$r_{\max} = S_{steer} + S_{brake} \quad (21)$$

The actual distance between vehicle and obstacle is recorded as d . If the actual distance is less than the influence range threshold ($d \leq r_{\max}$), the influence range will vary according to the safety distance. Otherwise, it will be reduced to the braking distance, realizing car following state between vehicles:

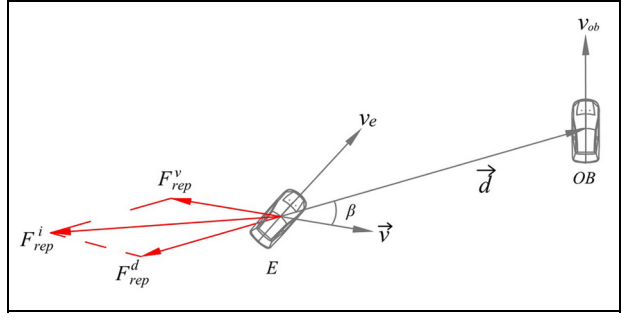


Figure 6. The improved repulsive force.

$$r = \begin{cases} S_{brake} + k_b \rho_0, & \beta \in (0, \theta] \cup [\pi - \theta, \pi) \quad d \leq r_{\max} \\ S_{steer} + k_s \rho_0, & \beta \in (\theta, \pi - \theta) \quad d \leq r_{\max} \\ S_{brake}, & \text{otherwise} \end{cases} \quad (22)$$

Improved repulsion

The effect of repulsion is to keep a relatively safe distance between the ego vehicle and other obstacles. In the traditional APF, since the repulsion is opposite to the relative position vector, the ego vehicle will be pushed away by it to realize collision avoidance. First of all, we introduce the threat level T_l based on different obstacles, indicating the degree of potential peril.³ In other words, if the ego vehicle enters the range of repulsion T_l will adjust. Otherwise, the threat level is zero, and the collision avoidance behaviour is not threatened.

$$T_l = \begin{cases} \lambda m_{ob} w_{ob} e^v, & d < r \\ 0, & \text{otherwise} \end{cases} \quad (23)$$

Where λ is the risk coefficient, m_{ob} is the mass of the obstacle, w_{ob} is the obstacle's width. Since the traditional repulsion is only related to the relative position, it is not suitable for dynamic traffic scenarios. For example, if the ego vehicle quickly approaches the obstacle, no sufficient repulsion generated to conduct the vehicle avoids the obstacle. By contrast, if the ego vehicle approaches the obstacle with a low relative speed, the computational cost increases and the operating efficiency is reduced. As a result, either situation may endanger traffic security. Therefore, the position repulsion F_{rep-p} and the speed repulsion F_{rep-v} are proposed in this paper.²² The former is related to the relative position and can prevent the vehicle from approaching the obstacle. The latter is opposite to the relative speed vector and decelerates the ego vehicle. Figure 6 shows the schematic diagram of the repulsive forces.

To establish the relationship between repulsion and velocity, the position repulsion coefficient k_{rep-p} can be defined as:

$$k_{rep-p} = k_{rp} \|\vec{v}\| \cos \beta \quad (24)$$

Where k_{rp} is a positive gain coefficient. In fact, in the case of the obstacle comes close to the vehicle ($\cos \beta > 0$) and the actual distance is less than the influence distance ($d < r$), the position repulsive force will start to act:

$$F_{rep}^d = \begin{cases} k_{rep-p} T_l \left(\frac{1}{d} - \frac{1}{r} \right) \frac{-\vec{d}}{\|\vec{d}\|}, & d < r \quad \cos \beta > 0 \\ 0, & otherwise \end{cases} \quad (25)$$

The speed repulsion coefficient can be expressed as follows:

$$k_{rep-v} = k_{rv} \|\vec{v}\| \quad (26)$$

Where k_{rv} is a positive gain coefficient, so the speed repulsion can be defined as:

$$F_{rep}^v = \begin{cases} k_{rep-v} T_l \left(\frac{1}{d} - \frac{1}{r} \right) \frac{-\vec{v}}{\|\vec{v}\|}, & d < r \\ 0, & otherwise \end{cases} \quad (27)$$

Through the parallelogram law, the total repulsion acting on the ego vehicle is synthesized by equations (25) and (27), improving the applicability in a dynamic environment:

$$F_{rep}^i = \begin{cases} \|\vec{v}\| T_l \left(\frac{1}{d} - \frac{1}{r} \right) (k_{rp} \cos \beta \frac{-\vec{d}}{\|\vec{d}\|} + k_{rv} \frac{-\vec{v}}{\|\vec{v}\|}), & d < r \\ 0, & otherwise \end{cases} \quad (28)$$

Where F_{rep}^i presents the total repulsion of the i -th obstacle to the ego vehicle. Within the influence distance r , equation (28) ensures that the faster the approaching speed of the obstacle or the smaller the actual distance d , the greater the repulsion to avoid the collision. Due to the existence of $\cos \beta$, if the vehicle comes close to the obstacle with a small relative angle, the vehicle will receive greater repulsion to plan a safe path.

Improved attraction

The attraction acts on the global area, and it can conduct the vehicle follow the planned path from the start point to the goal point, reaching the desired speed after avoiding the obstacle. In the traditional attraction construction, it only calculated the distance between the robot and the obstacle without considering the factor of speed between two objects, which cannot be suitable for a dynamic environment. In the paper, the attraction is divided into the global attraction F_{attg} and the speed attraction F_{attv} ; the former means:

$$F_{attg} = k_{attg} \rho_g \quad (29)$$

Where k_{attg} is the attractive coefficient, and ρ_g is the distance from the ego vehicle to the target point.

We consider the factor of speed and the improved repulsion within the range of r . The speed attraction is defined to increase the attraction at this moment appropriately.

$$F_{attv} = k_{attv} \|\vec{v}\| \rho_g \quad (30)$$

Where k_{attv} is the speed coefficient of attraction. When the actual distance is smaller than the influence distance, the speed attraction needs to work together with the global attraction. Otherwise, the ego vehicle towards the destination just under the effect of global attraction. So the attractive force on the ego vehicle is as follows:

$$F_{att} = \begin{cases} k_{attg} \rho_g + k_{attv} \|\vec{v}\| \rho_g, & d < r \\ k_{attg} \rho_g, & d \geq r \end{cases} \quad (31)$$

To sum up, the resultant force acting on the autonomous vehicle is as follows:

$$F = F_{road} + F_{rep}^i + F_{att} \quad (32)$$

Path tracking control

Generally, ensuring the ego vehicle follows the planned path with stable dynamics, the construction of a tracking controller is necessary. The section designs a lateral MPC controller and a longitudinal Fuzzy-PID controller to solve the tracking problem. The former is formulated as a constrained optimization based on the objective function and constraint conditions; the latter adjust and track the longitudinal speed through the accelerator pedal and the brake pedal.

Dynamics model

Since vehicle dynamics are very intricate in reality, and a high fidelity model is nonlinear,²¹ this paper ignores the steering system, the suspension system and the aerodynamic drag. We adopt the bicycle model of Ackerman steering to establish the vehicle dynamics model.³⁷

The bicycle model in Figure 7 contains the longitudinal, lateral and yaw degrees of freedom. According to Newton's second law, the vehicle motion equation can be expressed as:

$$\begin{aligned} m\ddot{x} &= m\dot{y}\dot{\phi} + 2F_{xf} + 2F_{xr} \\ m\ddot{y} &= -m\dot{x}\dot{\phi} + 2F_{yf} + 2F_{yr} \\ I_z\ddot{\phi} &= 2aF_{yf} - 2bF_{yr} \end{aligned} \quad (33)$$

Where F_{xf} and F_{xr} are the longitudinal forces on the front and rear tires, F_{yf} and F_{yr} are the lateral forces on the front and rear tires, I_z is the moment of inertia of the vehicle around the Z-axis, ϕ is the heading angle. In order to calculate the forces on tires, a linear Pacejka tire model is applied in this paper to solve the nonlinear problem.²⁴ The longitudinal and lateral force on the tire model can be presented as:

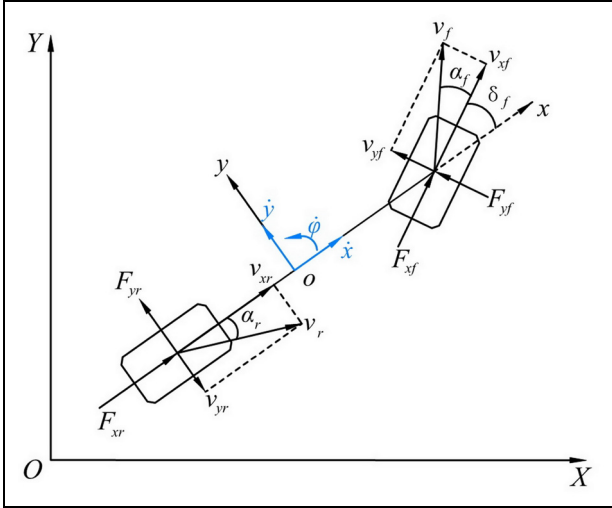


Figure 7. Vehicle dynamics model. XOY represents the earth coordinate system and xoy is the body coordinate system.

$$\begin{aligned} F_{xf} &= C_{xf} s_f \\ F_{yf} &= C_{yf} \alpha_f \\ F_{xr} &= C_{xr} s_r \\ F_{yr} &= C_{yr} \alpha_r \end{aligned} \quad (34)$$

Where C_{xf} and C_{xr} are longitudinal stiffness of the front and rear tires, respectively, C_{cf} and C_{cr} are lateral stiffness. s_f and s_r are the sideslip rates of tires, α_f and α_r are the sideslip angles. So, the vehicle dynamics model based on the assumption of linear tires and small front wheel angle is as follows:

$$\begin{aligned} m\ddot{y} &= -m\dot{x}\dot{\phi} + 2 \left[C_{yf} \left(\delta_f - \frac{\dot{y} + a\dot{\phi}}{\dot{x}} \right) + C_{yf} \frac{b\dot{\phi} - \dot{y}}{\dot{x}} \right] \\ m\ddot{x} &= m\dot{y}\dot{\phi} + 2 \left[C_{xf} s_f + C_{yf} \left(\delta_f - \frac{\dot{y} + a\dot{\phi}}{\dot{x}} \right) \delta_f + C_{xr} s_r \right] \\ I_z \ddot{\phi} &= 2 \left[a C_{yf} \left(\delta_f - \frac{\dot{y} + a\dot{\phi}}{\dot{x}} \right) - b C_{yr} \frac{b\dot{\phi} - \dot{y}}{\dot{x}} \right] \end{aligned} \quad (35)$$

The motion of the vehicle in the body coordinate system is converted to the earth coordinate system³⁸:

$$\begin{aligned} \dot{Y} &= \dot{x} \sin \phi + \dot{y} \cos \phi \\ \dot{X} &= \dot{x} \cos \phi - \dot{y} \sin \phi \end{aligned} \quad (36)$$

Lateral tracking controller

The establishment of the MPC controller contains the predictive model, objective function, and constraint conditions. Since the linear model predictive control has higher computational efficiency than the nonlinear one,³⁹ the linearized state-space equations are obtained as follows:

$$\begin{aligned} \dot{x}_l &= A x_l + B u \\ y_l &= C x_l \end{aligned} \quad (37)$$

Where the state-space vector is $x_l = [\dot{x}, \dot{y}, \phi, \dot{\phi}, X, Y]^T$, the front wheel angle is utilized as the control variable, and it is the input variable of this system $u = \delta_f$, A is the state matrix, B is the input matrix, and C is the output matrix, the output vector is $y_l = [\phi, Y]^T$.

The predictive model estimates the future output based on system information and control sequences. According to the Euler method,⁴⁰ the formula is discretely processed to obtain the predicted state-space equation:

$$\begin{aligned} \tilde{x}(t+1) &= A_t \tilde{x}(t) + B_t \Delta u(t) \\ \tilde{y}(t) &= C_t \tilde{x}(t) \end{aligned} \quad (38)$$

Where $\tilde{x}(t)$ is an expanded state-space variable which represents the current system information, Δu is the increment of the input variable, that is, $\Delta u = u(t) - u(t-1)$ and $u(t) = \delta_f(t)$, and A_t , B_t , C_t are the state matrix, input matrix, and output matrix in the discrete form.

Combining the deviation of the system and the optimization of the input variable, the objective function is to conduct the ego vehicle rapidly and smoothly track the planned path, which is defined as:

$$J(t) = \sum_{k=1}^{N_p} \left\| \tilde{y}_{t+k,t} - \tilde{y}_{ref_{t+k,t}} \right\|_Q^2 + \sum_{k=1}^{N_c-1} \left\| \Delta U_{t+k,t} \right\|_R^2 + \rho \varepsilon^2 \quad (39)$$

Where t is the current time, subscript $t+k, t$ presents the predicted value at k steps after t , N_p is the prediction horizon, N_c is the control horizon and $N_p > N_c$, y_{ref} is a reference matrix in N_p embracing the location of the planned path and the heading angle, ε is a slack variable to relax some constraints in case there are no viable solutions, Q and R are the weight matrices that indicate the capability of MPC to follow the planned path and the constraints of control variables, respectively; Furthermore, we assume that the input variable is held constant beyond N_c , ΔU is the predicted input increments before N_{c-1} steps.

According to Yang et al.,⁴¹ in the determination of the constraint conditions, the range of the control variable δ is $[-25^\circ, 25^\circ]$ and its increment $\Delta \delta$ is $[-9.4^\circ/s, 9.4^\circ/s]$, which must be constrained. The body sideslip angle β_y is one of the key factors to measure vehicle handling stability, so it needs to be limited to a rational range $[-12^\circ, 12^\circ]$. Besides, the dynamic performance of the automobile is not only affected by the driving force but also restricted by the adhesion condition. Since excessive lateral acceleration will affect comfort, the maximum constraint the acceleration in the lateral tracking controller is 0.4g:

$$\begin{aligned} \delta_{\min} &\leq \delta \leq \delta_{\max} \\ \Delta \delta_{\min} &\leq \Delta \delta \leq \Delta \delta_{\max} \\ \beta_{y\min} &\leq \beta_y \leq \beta_{y\max} \\ a_{y\min} &\leq a_y \leq a_{y\max} \end{aligned} \quad (40)$$

Integrating the objective function and constraints, the MPC tracking controller must solve the following optimization problems in each control cycle:

$$\begin{aligned}
 & \min_{\Delta U, \varepsilon} J(t) \\
 & \text{subj. to } \Delta U_{\min} \leq \Delta U \leq \Delta U_{\max} \\
 & \quad U_{\min} \leq A\Delta U + U(k-1) \leq U_{\max} \\
 & \quad y_{c\min} \leq y_c \leq y_{c\max} \\
 & \quad \varepsilon > 0
 \end{aligned} \tag{41}$$

Where A is a particular triangular matrix, y_c is the abovementioned constraint conditions. After each control cycle is solved, a sequence of the optimal input increments and the slack variable is obtained as follows:

$$\Delta U^* = [\Delta u^*(t), \Delta u^*(t+1), \dots, \Delta u^*(t+N_c-1), \varepsilon]^T \tag{42}$$

The first element of the sequence is applied, which acts as the controller's actual input increment.

$$u(k) = u(k-1) + \Delta u^*(k) \tag{43}$$

The MPC repeats the above process after entering the next cycle, realizing the tracking control of the desired path. The details of the matrix parameters and derivation process about MPC are given in Wang et al.²⁴

Longitudinal tracking controller

The vehicle is a complicated nonlinear system, and the longitudinal controller is to accurately track the desired speed through the accelerator pedal and the brake pedal. In a traditional PID controller, it cannot satisfy the online adjustment of parameter k_{p0} , k_{i0} , k_{d0} , which means it is unable to guarantee the stable control effect in a complicated environment.²⁵ Similar to applying in the ACC, the fuzzy method does not require an accurate model, and the control process can be effective.⁴² This paper uses fuzzy logic control to improve the traditional PID controller.

The architecture of the longitudinal tracking controller is the combination of a PID controller and a fuzzy controller. As shown in Figure 8, the difference between the desired speed v_x and the actual speed means the constantly changing error is used as an input variable. The signals of speed as output variables transmit to the vehicle dynamics model. In the established fuzzy-PID controller, the PID parameters k_p , k_i , and k_d are adjusted online and utilized by the fuzzy process according to the error e and the error rate e_c .

Active steering and the emergency braking are both options for obstacle avoidance. As described in Section II, if the distance condition is satisfied, the ego vehicle can avoid collision by changing lane, recorded as LC. Otherwise, it should decelerate and follow the front

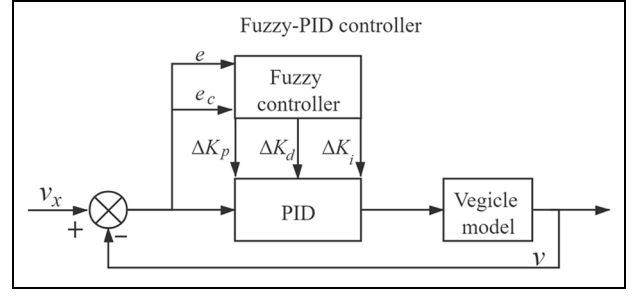


Figure 8. Fuzzy-PID tracking controller.

vehicle in the current lane, recorded as LK. Synthesizing the influence range of obstacles, the desired speed during collision avoidance can be expressed as:

$$v_x = \begin{cases} v_{ob} & \text{if } d \leq r, \text{LK} \\ v_e & \text{otherwise} \end{cases} \tag{44}$$

In other words, in free lane change or moving in a normal state, the expected speed should be based on the ego vehicle. When the autonomous vehicle enters the influence range r , if it fails to change lane and slow down to follow the participant ahead, the desired speed will be based on the obstacle in front of the current lane. Then the improved repulsive force and improved attractive force designed by this paper act to achieve safe path planning. Otherwise, it should be restored to the desired speed of car drivers.

Generally, the fuzzy process can be split into three phases: fuzzification, fuzzy inference and defuzzification. First, two input variables of the fuzzy controller are as follows:

$$\begin{aligned}
 e(t) &= v_x(t) - v(t) \\
 e_c(t) &= \frac{de(t)}{dt}
 \end{aligned} \tag{45}$$

Where $v_x(t)$ is the desired speed, $v(t)$ is the actual speed outputted from the vehicle dynamics model. This paper uses the incremental PID control theory, so the three output variables Δk_p , Δk_i , and Δk_d of the fuzzy controller is the increment of k_{p0} , k_{i0} , k_{d0} .

To realize the fuzzy PID control, first of all, find the fuzzy relation between two input variables and three output variables. We define e and e_c are varying in the range $[-6, 6]$, Δk_p , Δk_i , and Δk_d are varying in the range $[-2, 2]$, $[-0.6, 0.6]$, $[-0.03, 0.03]$. These five parameters are fuzzified into seven fuzzy sets by the fuzzy rulers according to the trigonometric functions: NB (negative big), NM (negative medium), NS (negative small), Z (zero), PS (positive small), PM (positive medium), P (positive big). The classical Mamdani method and the area centre method is used to solve fuzzy inference and defuzzification. The details of the whole process are in.²³ Therefore, the parameters of PID at the current time are recorded as:

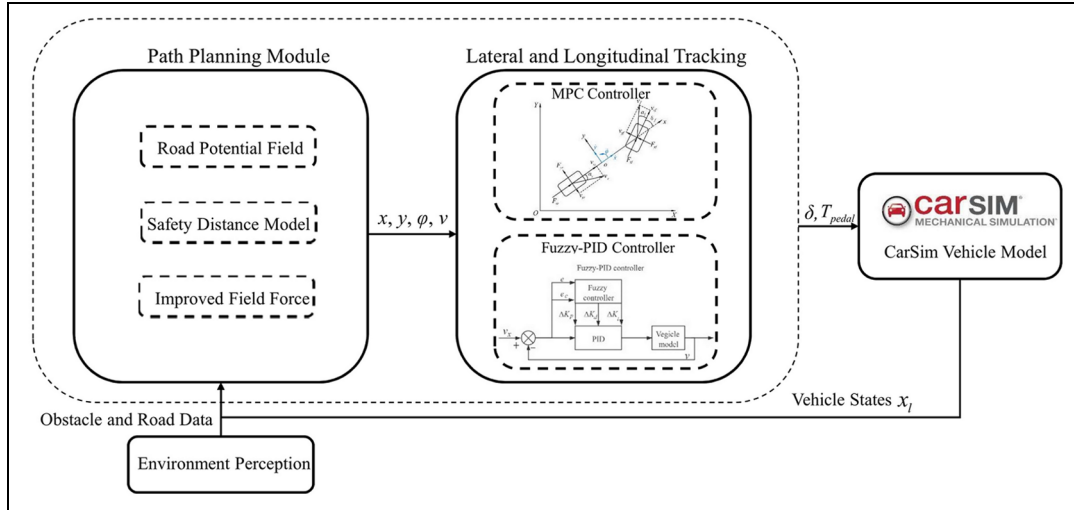


Figure 9. The architecture of co-simulation.

Table 1. Parameters of the algorithm and vehicle.

| Parameter | Description | Value |
|------------|--|-----------------------|
| t_0 | Driver response time (s) | 0.8 |
| a_{br} | Maximum braking deceleration of R (m/s^2) | 5.47 |
| d_0 | Ideal stopping clearance (m) | 3 |
| a_{be} | Maximum braking deceleration of E (m/s^2) | 5.47 |
| a_{ob} | Maximum braking deceleration of OB (m/s^2) | 5.47 |
| T_t | Time delay of the braking system (s) | 1 |
| k_{b1} | Coefficients of the left road boundary | 1 |
| k_{b2} | Coefficients of the right road boundary | 1 |
| k_c | Coefficient of the road centerline | 6.5 |
| σ_c | Convergence coefficient of road width | 0.5 |
| k_b | Distance coefficient | 1.6 |
| k_s | Distance coefficient | 1.5 |
| λ | Risk coefficient of obstacle | 1.18×10^{-8} |
| k_{rp} | Gain coefficient | 10 |
| k_{rv} | Gain coefficient | 12 |

$$\begin{aligned}
 k_p &= k_{p0} + \Delta k_p \\
 k_i &= k_{i0} + \Delta k_i \\
 k_d &= k_{d0} + \Delta k_d
 \end{aligned}
 \quad (46)$$

In reality, the speed should be converted into the resultant longitudinal force according to the vehicle model, calculating the throttle opening and brake pressure. To simplify the speed control model, the solver that comes with CarSim is used, which means that the fuzzy PID only tracks the speed signal of the car and sends it to the CarSim, completing the control of the corresponding pedal.

Simulation

At present, the sensors that a single smart car relies on are mainly radars and cameras. Besides, the vehicle-to-vehicle communication senses the vehicle status and shares them in real-time, which is an efficient complement to traditional perception methods.⁴³ This paper

only puts the primary emphasis on the path planning and tracking control level, and the intelligent vehicle can obtain the obstacle and road data through the onboard sensors and wireless communications.⁵ Three scenarios are simulated in the CarSim and Simulink environments to verify the feasibility of the proposed collision avoidance algorithm. In the constructed scenarios, the ego vehicle and obstacles select the C-class passenger cars that come with CarSim. The mass, velocity and maximum acceleration of participants are known. Figure 9 shows the architecture of co-simulation. Table 1 provides the relevant other parameters of the algorithm.

As shown in Figure 9, at each time step, once the environment is accurately perceived, the potential field and safety distance model are generated according to the road structure and surrounding cars, respectively. Then, the improved potential field force acts on the autonomous vehicle to generate the path based on the proposed algorithm. Meanwhile, according to the

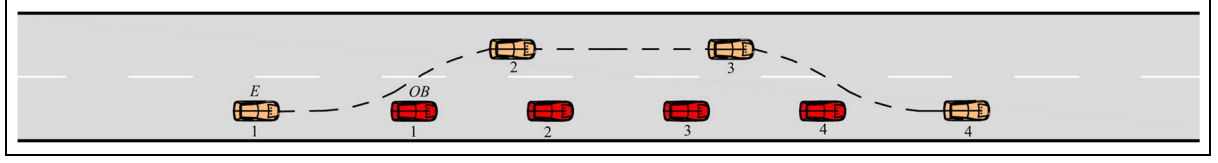


Figure 10. Demonstration of scenario 1.

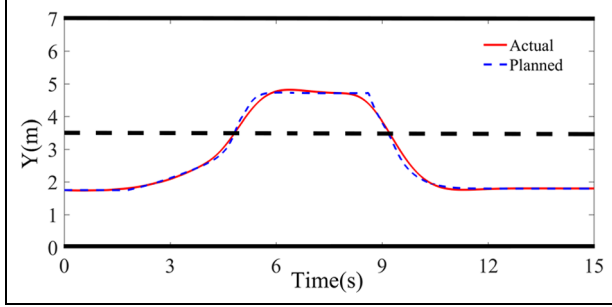


Figure 11. Planned path and actual path in Scenario 1.

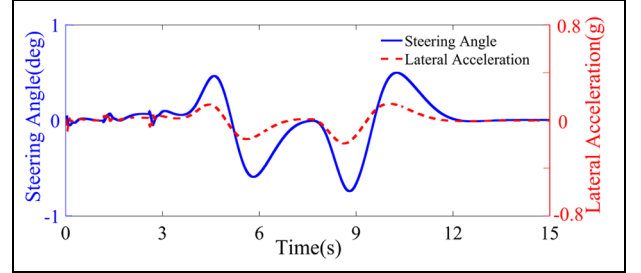


Figure 13. Steering angle and lateral acceleration in Scenario 1.

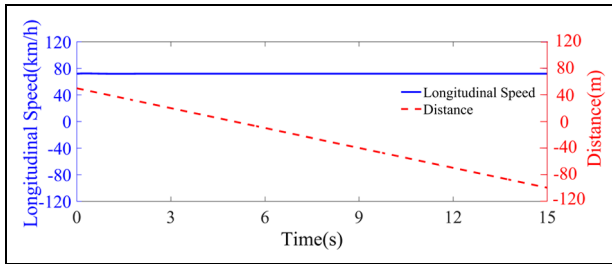


Figure 12. Longitudinal speed and distance in Scenario 1.

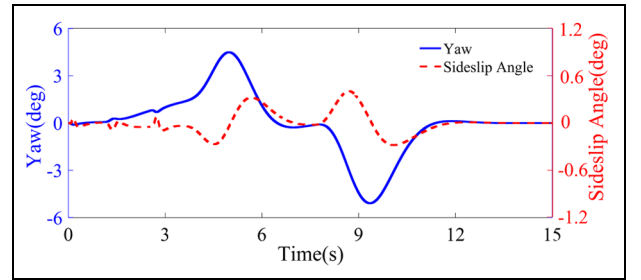


Figure 14. Yaw angle and sideslip angle in Scenario 1.

converted vehicle information (the state-space vector required by MPC and the vehicle speed required by Fuzzy-PID), the planned path is controlled by the lateral and longitudinal tracking module. Finally, the steering angle and pedal signals are transmitted to the CarSim vehicle model. During the co-simulation, the vehicle model also feeds the required vehicle status information x_i to the algorithm. This process is repeated at a fixed sample time and updated.

Scenarios I

Scenario 1 indicates the free lane-changing process. The ego vehicle is driving at 72 km/h, and the obstacle vehicle is moving slowly (36 km/h) simultaneously; the

original distance between them is 50 m. As shown in Figure 10, the ego vehicle E and the obstacle OB are indicated by orange and red, respectively. Furthermore, digital subscripts indicate the positions of cars at different sample times.

Since the initial distance is larger than S_{brakes} , and there are no other vehicles in the adjacent lane, E changes the lane as a collision-avoidance manoeuvre. The planned path and the actual trajectory shown in Figure 11 indicate that the tracking controller is satisfactory, and the trajectory is smooth. Due to the conventional algorithm cannot be applied in a dynamic environment. This paper designs a collision-avoidance path planning method based on the improved artificial

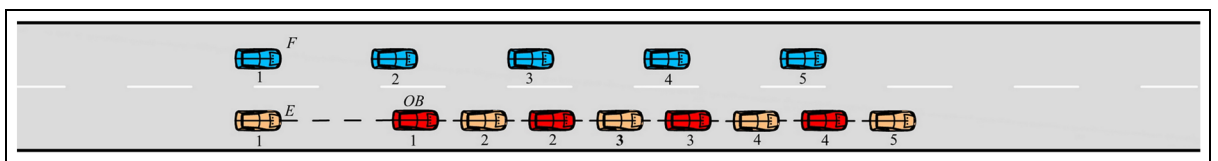


Figure 15. Demonstration of scenario 2.

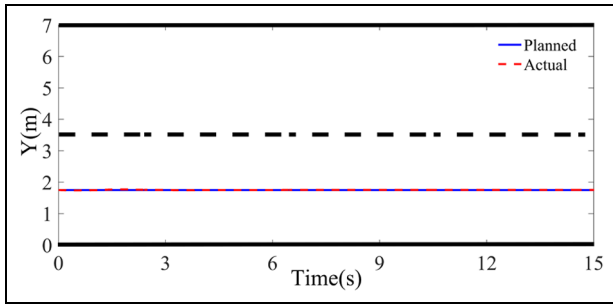


Figure 16. Planned path and actual path in Scenario 2.

potential field algorithm. It can be seen from the generated path that the proposed method can safely avoid dynamic obstacles. In Figure 12, the blue line shows the longitudinal speed, and the red dotted line is the real-time distance between *E* and *OB*. According to the simulation results, *E* starts to change lane at 35 m away from *OB*. Note that the distance value is zero at $t = 5$ s, which means *E* driving in the adjacent lane will overtake *OB* afterwards. At $t = 8$ s, *E* has crossed *OB* for 30 m, and it returns to the original lane. Compared with the traditional algorithm, in addition to the safety path generation. Figure 12 reflects the longitudinal distance between the vehicle and the obstacle, which proves that the controlled car can avoid collisions based on the safe distance.

Figure 13 shows the steering angle and the lateral acceleration. The maximum value of the lateral acceleration is $0.2g$, and the steering angle meets the constraint conditions, varying in the range of $\pm 1^\circ$. In terms of stability, as shown in Figure 14, during the whole process of changing lane, the yaw curve is smooth, and it always varies in the range of $\pm 6^\circ$. The tire sideslip angle value is small and can constrain the tires within the linear area. To conclude, the proposed algorithm can generate a collision-free path and ensure that the collision avoidance process keeps comfort and stability.

Scenarios2

As shown in Figure 15, Scenario 2 demonstrates the car-following state during traffic collision avoidance. The orange car *E* moves at 72 km/h, and the red obstacle *OB* is driving at 36 km/h in the same lane with an initial distance of 50 m. In the left lane, the blue car *F* moves at 36 km/h. In this case, since the left lane does not have enough space to accommodate *E* (the real-time distance between *E* and *F* is always less than S_r), *E* will not complete the collision avoidance manoeuvre by changing lane; it will decrease the speed to follow *OB*.

Since the local optimal problem, the traditional APF algorithm is easy to stop running in scenario 2 (the attractive force and repulsive force are equal and opposite). However, as shown in Figure 16, the planned path

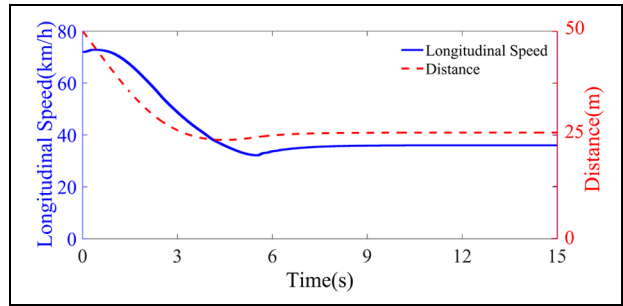


Figure 17. Longitudinal speed and distance in Scenario 2.

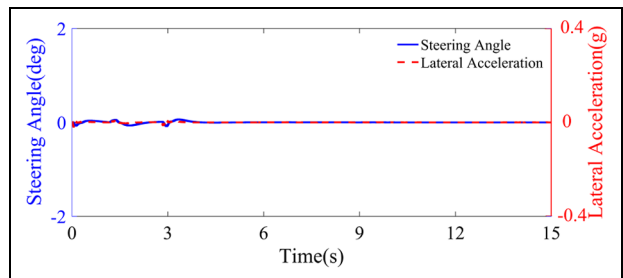


Figure 18. Steering angle and lateral acceleration in Scenario 2.

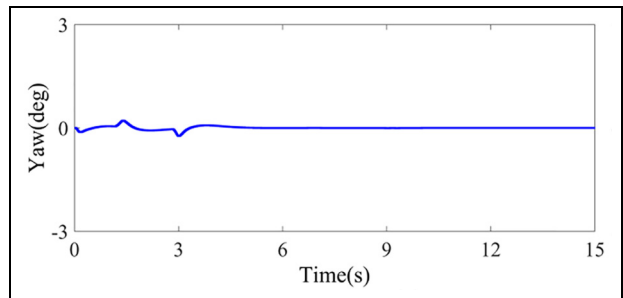


Figure 19. Yaw angle in Scenario 2.

and the actual trajectory are continuous without oscillation based on the improved APF method. When collision avoidance fails to be achieved by steering, the proposed algorithm is more flexible than the traditional method, and it can adaptively follow the preceding vehicle. Figure 17 is the real-time distance curve between *E* and *OB*, and the longitudinal speed change is also presented in it. The simulation results show that *E* decelerates to the same speed as *OB* and ultimately keeps an appropriate distance (26 m) moving together, maintaining safety performance with *E*. The built-in distance model and the improved potential field force of the proposed algorithm realizing the movement state under the safe distance conditions.

In Figure 18, the steering angle and the lateral acceleration are almost zero, indicating straight driving performance. As shown in Figure 19, the yaw curve is smooth and small to keep stability; it only varies in the $\pm 1^\circ$ range.

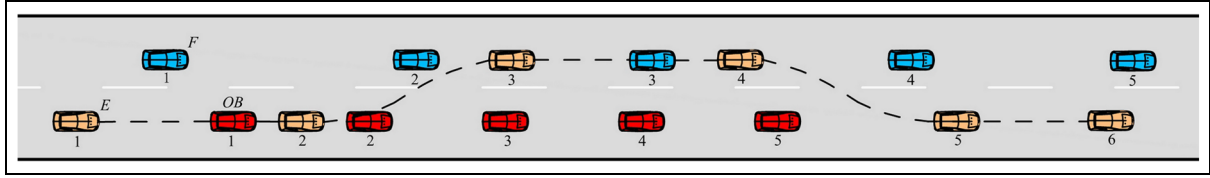


Figure 20. Demonstration of Scenario 3.

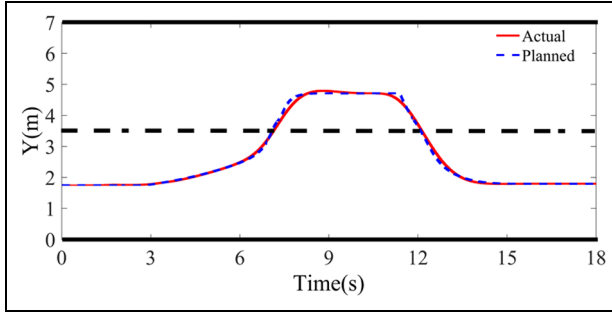


Figure 21. Planned path and actual path in Scenario 3.

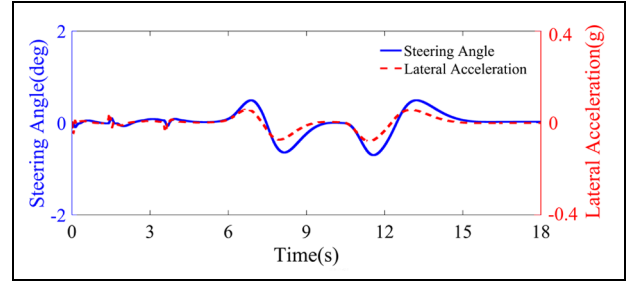


Figure 23. Steering angle and lateral acceleration in Scenario 3.

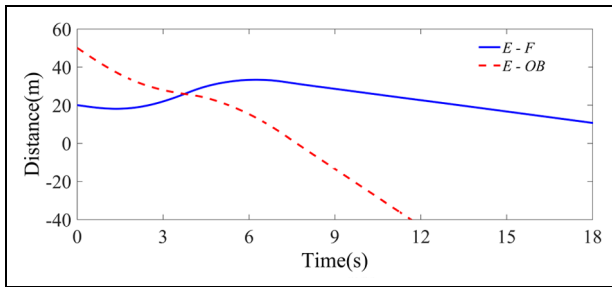


Figure 22. Distance curve in Scenario 3, $E-F$ represents the longitudinal distance between the ego vehicle and the front vehicle, $E-OB$ represents the longitudinal distance between the ego vehicle and the obstacle in the current lane, the negative value means E has overtaken OB .

Scenarios3

Figure 20 shows Scenario 3, which is similar to Scenario 1. The orange car E is driving at 72 km/h, and the red obstacle OB is moving slowly (36 km/h) in the identical lane. The original distance between them is 50 m. In the adjacent lane, the side vehicle F is 20 m in front of E , and its speed is 64.8 km/h. Besides the ability to freely change lane and adaptively follow the leading vehicle, the improved algorithm should also reflect the performance to deal with the mixed situation of the former two scenarios.

As shown in Figure 21, the path is smooth and continuous. In this case, since the initially real-time distance between E and F is less than S_f (the value is 21 m in Scenario 3), E first decreases the speed to keep a safe longitudinal distance with OB . In Figure 22, the red curve represents the real-time distance between E and

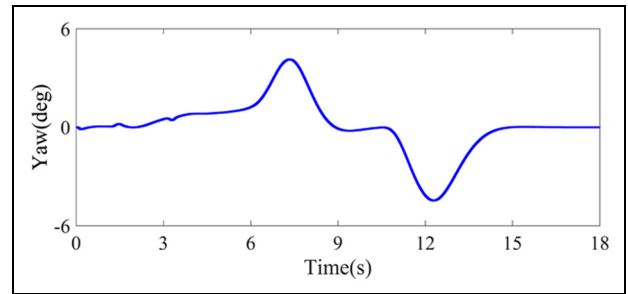


Figure 24. Yaw angle in Scenario 3.

OB , and the blue curve is the real-time distance between E and F . At $t = 3$ s, since the blue curve value is 22 m (it is greater than S_f), the spacing condition is met, and E switches lane at this time. After driving in an adjacent lane, F will become a new obstacle, and E returns to the original lane at $t = 11$ s (the red curve shows it has crossed OB for 33 m). Figure 23 shows the steering angle within $\pm 1^\circ$. The lateral acceleration is < 0.4 g, which meets the constraint conditions. In Figure 24, the curve is smooth and always varies in the range of $\pm 6^\circ$. During the safe collision avoidance process, the ego vehicle can maintain stability and comfort.

Conclusion

To plan a safe path on traffic roads without affecting other surrounding cars. This paper proposes the collision avoidance algorithm based on the improved artificial potential field algorithm. The proposed path planning method uses the safety distance model to improve the influence range of obstacles, allowing the

automated vehicle to perform the corresponding avoidance manoeuvres in simulated traffic scenarios. Furthermore, combine the MPC controller with the Fuzzy-PID controller to track longitudinal and lateral motion to ensure comfort and stability for the vehicle. The proposed collision avoidance method has been simulated in three scenarios, showing the performance in freely changing lane, adaptively following the leading vehicle, and processing in a mixed situation. The results demonstrate the performance of lane-keeping braking and lane-changing stability, generating safe and driver-like trajectories in real-time.

Compared with the conventional APF algorithm, the improved artificial potential field algorithm proposed in this paper can plan an appropriate collision avoidance path under safe distance conditions, and the response parameters also meet the stability requirements. However, this paper introduced the mass and the maximum acceleration factors of participants, assigned the values in the simulated scenarios to verify the proposed collision avoidance method. Furthermore, the perception module actually impacts planning and tracking levels, so how to evaluate parameters uncertainty in a dynamic environment and the impact of numerical changes would be another challenge in our future research. The non-crossable obstacles (e.g. pedestrian and road depression) and the crossable obstacles (e.g. vehicle) will confuse the algorithm. Future research will further explore these complicated cases and predict trajectories of objects.




Declaration of conflicting interests

The author(s) declared no potential conflicts of interest with respect to the research, authorship, and/or publication of this article.

Funding

The author(s) disclosed receipt of the following financial support for the research, authorship, and/or publication of this article: This work was supported in part by the National Key Research and Development Project (Study on operation safety and defect characteristics of NEVs and construction of its characterization system) under Grant 2020YFB1600601, the Power Battery Thermal Runaway Defect Analysis and Fire Depth Investigation Technology Research under Grant 282020Y-7510, and the National Automobile Accident In-Depth Investigation System -NAIS.

ORCID iDs

Song Feng  <https://orcid.org/0000-0002-8397-2440>
Yubin Qian  <https://orcid.org/0000-0002-3986-5330>
Yan Wang  <https://orcid.org/0000-0001-7066-6797>

References

1. Ba Y, Zhang W, Wang Q, et al. Crash prediction with behavioral and physiological features for advanced vehicle collision avoidance system. *Transp Res Part C Emerg Technol* 2017; 74: 22–33.
2. Yang K, Guler SI and Menendez M. Isolated intersection control for various levels of vehicle technology: conventional, connected, and automated vehicles. *Transp Res Part C Emerg Technol* 2016; 72: 109–129.
3. Wang P, Gao S, Li L, et al. Obstacle avoidance path planning design for autonomous driving vehicles based on an improved artificial potential field algorithm. *Energies* 2019; 12: 2342–2355.
4. Gallagher B, Akalsuka H and Suzuki H. Wireless communications for vehicle safety: radio link performance and wireless connectivity methods. *IEEE Veh Technol Mag* 2006; 1: 4–24.
5. Huang Z, Chu D, Wu C, et al. Path planning and cooperative control for automated vehicle platoon using hybrid automata. *IEEE Trans Intell Transp Syst* 2019; 20: 959–974.
6. Saravanakumar S and Asokan T. Multipoint potential field method for path planning of autonomous underwater vehicles in 3D space. *Intell Serv Robot* 2013; 6: 211–224.
7. Ferguson D and Stentz A. Anytime, dynamic planning in high-dimensional search spaces. In: *Proceedings IEEE international conference on robotics and automation*, Rome, Italy, 10–14 April 2007, pp.1310–1315. New York: IEEE.
8. Urmson C and Whittaker W. Self-driving cars and the urban challenge. *IEEE Intell Syst* 2008; 23: 66–68.
9. Pang Y, Song Z, Li X, et al. Truncation error analysis on reconstruction of signal from unsymmetrical local average sampling. *IEEE Trans Cybern* 2015; 45: 2100–2104.
10. Moon C and Chung W. Kinodynamic planner dual-tree RRT (DT-RRT) for two-wheeled mobile robots using the rapidly exploring random tree. *IEEE Trans Ind Electron* 2015; 62: 1080–1090.
11. Lan X and Cairano SD. Continuous curvature path planning for semi-autonomous vehicle maneuvers using RRT. In: *European control conference (ECC)*, Linz, Austria, 15–17 July 2015, pp.2360–2365. New York: IEEE.
12. Shi Y, Li Q, Bu S, et al. Research on intelligent vehicle path planning based on rapidly-exploring random tree. *Math Probl Eng* 2020; 2020: 1–14.
13. Lin Y and Saripalli S. Sampling-based path planning for UAV collision avoidance. *IEEE Trans Intell Transp Syst* 2017; 18: 3179–3192.
14. Piazzi A, Bianco CGL, Bertozzi M, et al. Quintic G/sup 2/-splines for the iterative steering of vision-based autonomous vehicles. *IEEE Trans Intell Transp Syst* 2002; 3: 27–36.
15. Hamann B, Wu D and Moorhead RJ. On particle path generation based on quadrilinear interpolation and Bernstein-Bezier polynomials. *IEEE Trans Vis Comput Graph* 1995; 1: 210–217.
16. Zhang S, Simkani M and Zadeh MH. Automatic vehicle parallel parking design using fifth degree polynomial path

- planning. In: *IEEE vehicular technology conference (VTC Fall)*, San Francisco, CA, 5–8 September 2011, pp.1–4. New York: IEEE.
17. Bing H, Gang L, Jiang J, et al. A route planning method based on improved artificial potential field algorithm. In: *IEEE 3rd international conference on communication software and networks*, Xi'an, China, 27–29 May 2011, pp.550–554. New York: IEEE.
 18. Raja R, Dutta A and Venkatesh KS. New potential field method for rough terrain path planning using genetic algorithm for a 6-wheel rover. *Robot Auton Syst* 2015; 72: 295–306.
 19. Gao K, Yan D, Yang F, et al. Conditional artificial potential field-based autonomous vehicle safety control with interference of lane changing in mixed traffic scenario. *Sensors* 2019; 19: 4199.
 20. Ji J, Khajepour A, Melek WW, et al. Path planning and tracking for vehicle collision avoidance based on model predictive control with multiconstraints. *IEEE Trans Veh Technol* 2017; 66: 952–964.
 21. Huang Y, Ding H, Zhang Y, et al. A motion planning and tracking framework for autonomous vehicles based on artificial potential field elaborated resistance network approach. *IEEE Trans Ind Electron* 2020; 67: 1376–1386.
 22. Du Y, Zhang X and Nie Z. A real-time collision avoidance strategy in dynamic airspace based on dynamic artificial potential field algorithm. *IEEE Access* 2019; 7: 169469–169479.
 23. Shim T, Adireddy G and Yuan H. Autonomous vehicle collision avoidance system using path planning and model-predictive-control-based active front steering and wheel torque control. *Proc IMechE, Part D: J Automobile Engineering* 2012; 226: 767–778.
 24. Wang H, Liu B, Ping X, et al. Path tracking control for autonomous vehicles based on an improved MPC. *IEEE Access* 2019; 7: 161064–161073.
 25. Lihan S, Jie M and Baoqing Y. Fuzzy PID design of vehicle attitude control systems. In: *Chinese control and decision conference (CCDC)*, Hefei, China, 22–24 August 2020, pp.1826–1830. New York: IEEE.
 26. Wang J, Zheng H and Zong C. Longitudinal and lateral dynamics control of automatic lane change system. *Trans Inst Meas Control* 2019; 41: 4322–4338.
 27. Cao H, Song X, Huang Z, et al. Simulation research on emergency path planning of an active collision avoidance system combined with longitudinal control for an autonomous vehicle. *Proc IMechE, Part D: J Automobile Engineering* 2016; 230: 1624–1653.
 28. Wang W, Huang Y, Khajepour A, et al. Crash mitigation in motion planning for autonomous vehicles. *IEEE Trans Intell Transp Syst* 2019; 20: 3313–3323.
 29. Hassanzadeh M, Lidberg M, Keshavarz M, et al. Path and speed control of a heavy vehicle for collision avoidance maneuvers. In: *IEEE intelligent vehicles symposium*, Alcalá de Henares, Madrid, Spain, 3–7 June 2012, pp.129–134. New York: IEEE.
 30. Wang C, Sun Q, Li Z, et al. Human-like lane change decision model for autonomous vehicles that considers the risk perception of drivers in mixed traffic. *Sensors* 2020; 20: 2259.
 31. Moon S and Yi K. Human driving data-based design of a vehicle adaptive cruise control algorithm. *Veh Syst Dyn* 2008; 46: 661–690.
 32. Chae H and Yi K. Virtual target-based overtaking decision, motion planning, and control of autonomous vehicles. *IEEE Access* 2020; 8: 51363–51376.
 33. Yuan C, Weng S, Shen J, et al. Research on active collision avoidance algorithm for intelligent vehicle based on improved artificial potential field model. *Int J Adv Robot Syst* 2020; 17: 1729881420911232.
 34. Khatib O. Real-time collision avoidance for manipulators and mobile robots. *Int J Rob Res* 1986; 5: 90–98.
 35. Ragland C and Dalrymple G. Overlap car-to-car tests compared to car-to-half barrier and car-to-full barrier tests. *Auto Traffic Saf* 1994; 1: 22–30.
 36. Furuichi H, Huang J, Fukuda T, et al. Switching dynamic modeling and driving stability analysis of three-wheeled narrow tilting vehicle. *IEEE Trans Vis Comput Graph* 2014; 19: 1309–1322.
 37. Gupta A, Divekar R and Agrawal M. Autonomous parallel parking system for Ackerman steering four wheelers. In: *IEEE international conference on computational intelligence and computing research*, Coimbatore, India, 28–29 December 2010, pp.1–6. New York: IEEE.
 38. Juan A, Cabrera Juan J, et al. A procedure for determining tire-road friction characteristics using a modification of the magic formula based on experimental results. *Sensors* 2018; 18: 896.
 39. Sun C, Zhang X, Zhou Q, et al. A model predictive controller with switched tracking error for autonomous vehicle path tracking. *IEEE Access* 2019; 7: 53103–53114.
 40. Huang Y, Khajepour T, Zhu T, et al. A supervisory energy-saving controller for a novel anti-idling system of service vehicles. *IEEE ASME Trans Mechatron* 2017; 22: 1037–1046.
 41. Yang X, Lu L, Chu D, et al. Unified modeling of trajectory planning and tracking for unmanned vehicle. *Acta Autom Sin* 2019; 45: 799–807.
 42. Kodagoda KRS, Wijesoma WS and Teoh EK. Fuzzy speed and steering control of an AGV. *IEEE Trans Control Syst Technol* 2002; 10: 112–120.
 43. Ammoun S and Nashashibi F. Design and efficiency measurement of cooperative driver assistance system based on wireless communication devices. *Transp Res Part C Emerg Technol* 2010; 18: 408–428.